

METAPLEX NETWORKS: INFLUENCE OF THE EXO-ENDO STRUCTURE OF COMPLEX SYSTEMS ON DIFFUSION*

ERNESTO ESTRADA[†], GISSELL ESTRADA-RODRIGUEZ[‡], AND HEIKO GIMPERLEIN[‡]

Abstract. In a complex system the interplay between the internal structure of its entities and their interconnection may play a fundamental role in the global functioning of the system. Here, we define the concept of metaplex, which describes such trade-off between internal structure of entities and their interconnections. We then define a dynamical system on a metaplex and study diffusive processes on them. We provide analytical and computational evidences about the role played by the size of the nodes, the location of the internal coupling areas, and the strength and range of the coupling between the nodes on the global dynamics of metaplexes. Finally, we extend our analysis to two real-world metaplexes: a landscape and a brain metaplex. We corroborate that the internal structure of the nodes in a metaplex may dominate the global dynamics (brain metaplex) or play a regulatory role (landscape metaplex) to the influence of the interconnection between nodes.

Key words. Complex networks, metaplex network, d -path Laplacian, diffusion

AMS subject classifications. 05C81, 92C99, 35P05, 47G99

1. Introduction. A complex system is characterized by the existence of many components which are interdependent on each other [20, 40, 49]. Each of these components is at the same time characterized by certain structure, dynamics and function [4], which influences the global behaviour of the system. The interconnection between these components represents the exo-skeleton of the complex system, and it is well characterized by the use of complex networks [20, 40, 49]. The internal structure of the corresponding entities – inside the nodes of the complex network – represents the endo structure of the system and it is not necessarily a network in itself. Let us consider some examples, from the vast variety that exists in nature and society, to illustrate the point.

The first type of systems, represented in Figure 1a, is formed by cells which are interconnected by means of their physical contacts, such as in the case of cellular systems in tissues, neuronal networks or astrocytic complexes, i.e., star-shaped glial cells [48]. In this case the exo-skeleton of the system is the cellular network *per se*, and their endo-skeleton is described by the crowded environment inside the cells, where up to 40% of the cytoplasmic volume is occupied by RNA, ribosomes and proteins [69, 70]. The situation is similar if we consider regions inside an organ instead of individual cells. A typical example is the consideration of anatomical or functional regions of the brain [8]. Here again the system is characterized by an exo-skeleton formed by the brain network and an endo-structure describing the interior of those regions.

In the second example illustrated in Figure 1b we consider an enriched conceptual

*Submitted to the editors.

Funding: G. E. R. was supported by The Maxwell Institute Graduate School in Analysis and its Applications, a Centre for Doctoral Training funded by the UK Engineering and Physical Sciences Research Council (grant EP/L016508/01), the Scottish Funding Council, Heriot-Watt University and the University of Edinburgh.

[†]Institute of Applied Mathematics (IUMA), Universidad de Zaragoza, Pedro Cerbuna 12, E-50009 Zaragoza, Spain; ARAID Foundation, Government of Aragón, E-50018 Zaragoza, Spain; and Instituto de Ciencias Matematicas e de Computacao, Universidade de Sao Paulo, Caixa Postal 668, 13560-970 Sao Carlos, Sao Paulo, Brazil (estrada66@unizar.es).

[‡]Maxwell Institute for Mathematical Sciences and Department of Mathematics, Heriot-Watt University, Edinburgh, EH14 4AS, United Kingdom (ge5@hw.ac.uk, h.gimperlein@hw.ac.uk.)

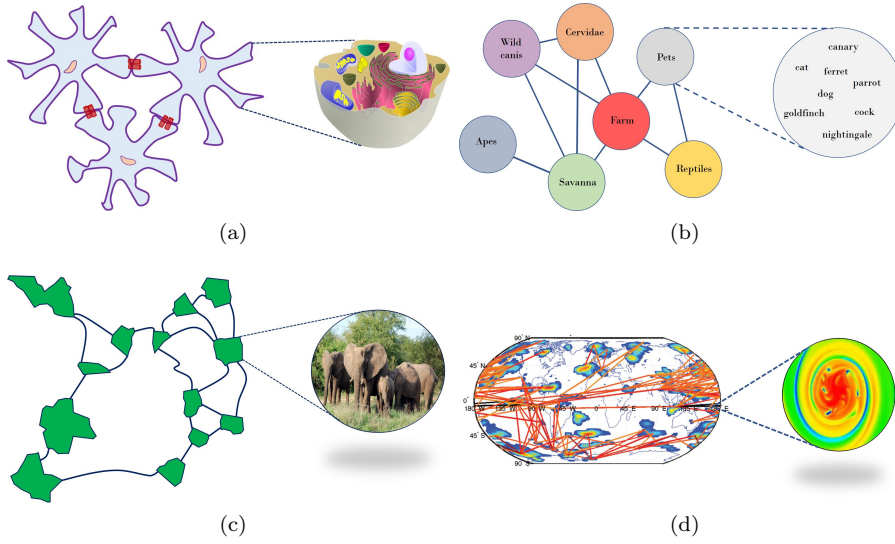


FIG. 1. (a) Illustration of a cellular system formed by biological cells connected by means of gap junctions to interchange chemicals and a zoom of the internal structure of a cell. (b) Enriched conceptual system representing the conceptual organization of animal categories. (c) Landscape ecological system formed by patches interconnected by corridors used by some species to move from patch to patch. Zooming-in reveals the foraging movement of these species inside the patches. (d) Climate system formed by a network of climatic events correlations and the internal climatic events at local regions.

metaplex. This is a conceptual organization model inferred by Goñi et al. [31] from verbal fluency of 200 individuals. The study was aimed at finding the conceptual storage structure of the natural category of animals as a network. Thus, every node of the metaplex represents a category of animals, e.g., pets, and inside the nodes we find all the words in that category.

Our third example consists of the patches formed in an ecological landscape as illustrated in Figure 1c. In this case, the system of patches and the corridors connecting them forms an exo-skeleton known as a landscape network [63]. The combination of the geographic and ecological features of the individual patches determine their endo-structures. This example will be discussed hereafter in this work.

The final example is however at a much larger scale (see Figure 1d). It corresponds to a climate system in which the nodes represent geographical regions in the world. These regions are connected by climatic correlations or causalities, such that two regions are connected if a climatic event in one region triggers a climatic event in the other [67, 15]. Inside every region, however, there is a vast collection of complex phenomena taking place which are typically modeled by using weather and local climatic models.

A common dynamical process taking place in the systems described in Figure 1 is diffusion, which is also ubiquitous in many other physical [26], chemical [38], biological and socio-economic systems [35, 41], especially on mesoscopic scales [68]. In the systems described before, as well as in many other complex systems, there is a trade-off between a diffusive process taking place inside the entities of the systems and the diffusion taking place between them. When both, the endo- and the exo-structure of the complex system are representable by networks we can use some of the physico-

mathematical tools already available in the literature, such as networks of networks [27, 59] or multiplexes [3, 30, 36, 55]. However, the main challenge here is that in many occasions the endo-structure of the system is described by a continuous space while the exo-skeleton is a discrete one, e.g., a network. In the case of cells, their interior is formed mainly by cytoplasm which is formed by 80% of water [43], while their interconnection is well described by a cellular network. Goñi et al. [31] considered in their work that inside each category every pair of words were connected. Thus, it is assumed that the internal space inside categories is a continuum in which words are found in a random-walk-like navigation inside the memory of individuals. In the next example, where species are moving in a patchy environment, the movement inside the patches is better described by using continuous diffusive models [1, 9], and the hop between patches through the narrow corridors is better accounted for by using a network-theoretic approach [63]. Finally, in climate systems the processes inside the regions – nodes – are well described by aerodynamics and fluid dynamics, while the causal influence between regions is well described by a network of interactions, including long range effects [15, 67].

The implications of this endo-exo trade-off in complex systems is very important for understanding their functioning. There is experimental evidence, for instance, that the movement of small molecules inside a cell follows an anomalous diffusive processes, either subdiffusive [29, 51, 65] or superdiffusive [56]. The distinction between normal (or Fickian) and anomalous diffusion is made on the basis of the scaling of the mean squared displacement $\langle x^2 \rangle = \langle (x - x_0)^2 \rangle$ of the diffusive particle with time [7, 46], where x is the current position of a particle and x_0 is the initial position. See Supplementary Information for a more detailed description of anomalous diffusion. While for normal diffusion the mean squared displacement scales linearly with time $\langle x^2 \rangle \sim t$, for anomalous diffusion it scales as a power-law $\langle x^2 \rangle \sim t^\alpha$, with exponent $\alpha \in (0, 2)$ larger (super-) or smaller (sub-) than one. This means that on long time scales in a superdiffusive process the space explored by the diffusive particle is larger than the one explored in a normal diffusion in exactly the same time, due to a high probability of long range hopping. In the case of a small molecule inside a cell, the anomalous diffusion is mainly due to the crowded environment inside the cells [58, 60]. However, there are more complex mechanisms inside certain types of cells that can lead to anomalous diffusive processes. An example is the generation of calcium waves [10] which have been observed in cardiac muscle [25], in skeletal muscle fibre [16], medaka eggs [57] and astrocytes [11]. This subdiffusive Ca^{2+} movement may be involved with cardiac [39, 42] and brain diseases [66, 34].

When global systems, such as tissues [50] or the whole brain [8], are analyzed, superdiffusive processes have been experimentally observed for fresh specimen of carcinoma, fibrous mastopathies, adipose and liver tissues [37] as well as for signals navigating across regions of the brain [12]. Interesting research questions emerge from these experiments: Is the anomalous diffusive behavior of a global system the consequence of sub or superdiffusive processes inside the entities, e.g., cells or regions? Are they the result of the anomalous diffusion between the entities only? Is it the combination of the exo- and endo-structures which determines the nature of the diffusive process in a complex system? How relevant is the endo-structure depending on the type of network, i.e. small-world network? Similar questions emerge for the analysis of other systems, such as the landscape system discussed above. In landscape systems the superdiffusive movement of species inside a patch is well documented and described by continuous models [1, 9, 64]. Can this behavior alone determine the nature of the diffusive process at the global landscape level?

In this work we answer these questions by introducing the concept of *metaplexes*. Informally, a metaplex is a representation of a complex system in which the internal structure of the nodes and the interconnection between them are considered at the same time (see Figure 2). Thus, a dynamical system on a metaplex consists of the coupling between the dynamics inside the entities, typically a continuous space, and the dynamics between these entities which is controlled by the inter-entity connectivity.

Our results show that in a linear metaplex, superdiffusion due to long range hopping in a network, as in [22], survives irrespective of the internal structure of the nodes. On the other hand, we prove that superdiffusion in the nodes can speed up regular diffusion in the metaplex, but it cannot lead to superdiffusion. The geometry of the nodes and their coupling play crucial roles for the global dynamics, which we explain in a combination of analysis and numerical experiments. The results shed light on the rich and substantially different nature of the dynamics of metaplexes and the interplay of their exo- and endo-structure, also in the real-world systems considered in Subsection 6.3.1.

Here we start by a formal definition of a metaplex and a dynamical system on it. We then study a linear toy model that allows us to understand some of the fundamental principles of diffusive processes on metaplexes. Finally, we study two real-world metaplexes pointing at the potential applications of this representation of complex systems.

2. Preliminaries. In this section we define the concepts and settle the notation to be used in this work. Here we consider two kinds of diffusive dynamical systems, one taking place in a continuous space and the other in a discrete one. Let us start by defining the diffusive process on the continuous space.

Let $u(t, \mathbf{x})$ be the density of the diffusive particle at time t for \mathbf{x} in a domain in \mathbb{R}^n . The density $u(t, \mathbf{x})$ evolves according to

$$(2.1) \quad \partial_t u(t, \mathbf{x}) = (-\Delta)^s u(t, \mathbf{x}),$$

where $(-\Delta)^s$ denotes a *fractional Laplacian operator* for $s \in (0, 1]$. The application of the fractional Laplacian to $u(t, \mathbf{x})$ on \mathbb{R}^n at a fixed time t is given by

$$(2.2) \quad (-\Delta)^s u(\mathbf{x}) = c_{n,s} P.V. \int_{\mathbb{R}^n} \frac{u(\mathbf{x}) - u(\mathbf{y})}{|\mathbf{x} - \mathbf{y}|^{n+2s}} d\mathbf{y} = c_{n,s} \lim_{\varepsilon \rightarrow 0^+} \int_{\{|\mathbf{y}| > \varepsilon\}} \frac{u(\mathbf{x}) - u(\mathbf{y})}{|\mathbf{x} - \mathbf{y}|^{n+2s}} d\mathbf{y},$$

where $P.V.$ denotes the Cauchy principal value, and $c_{n,s}$ is the following normalization

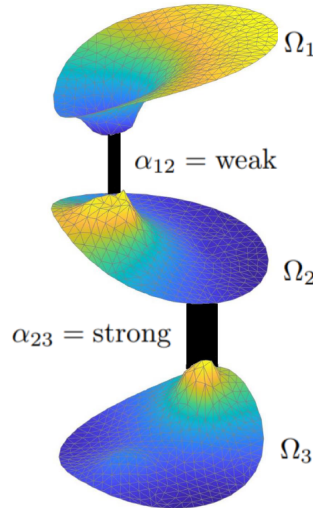


FIG. 2. *Diffusion in a metaplex.* The domains Ω_j are the nodes of the graph (exo-skeleton) in which a continuous diffusion process takes place. The connections with different strengths, given by α_{12} and α_{23} , account for the edges of the graph. The colours indicate the "density" of the diffusing particles, with yellow for higher concentration.

constant in terms of Euler Gamma functions

$$c_{n,s} = \frac{2^{2s} s \Gamma\left(\frac{n+2s}{2}\right)}{\pi^{\frac{n}{2}} \Gamma(1-s)}.$$

In a domain $\Omega \subset \mathbb{R}^n$ it is better to define the fractional Laplacian in terms of the following bilinear form:

$$(2.3) \quad \int_{\Omega} (-\Delta)^s u(\mathbf{x}) v(\mathbf{x}) d\mathbf{x} = \frac{c_{n,s}}{2} \iint_{(\Omega \times \mathbb{R}^n) \cup (\mathbb{R}^n \times \Omega)} \frac{(u(\mathbf{x}) - u(\mathbf{y}))(v(\mathbf{x}) - v(\mathbf{y}))}{|\mathbf{x} - \mathbf{y}|^{n+2s}} d\mathbf{y} d\mathbf{x},$$

for u, v belonging to the Sobolev space $H^s(\Omega)$. When $s = 1$ this operator corresponds to the differential Laplacian operator $\Delta u = \partial_{x_1}^2 u + \dots + \partial_{x_n}^2 u$ [46, 47] with Neumann boundary conditions [14].

Let us now move on to the diffusive process on a discrete space. Let $G = (V, E)$ be a simple, connected graph with $|V| = N$ nodes and $|E| = m$ edges. The degree of a node in V is the number of its nearest neighbors. Let $\text{dist}(v, w)$ be the shortest path distance between the nodes $v \in V$ and $w \in V$, i.e., the number of edges in one shortest path connecting both nodes. Let $d_{max} = \max_{v,w} \text{dist}(v, w)$ be the maximum distance between any pair of nodes in G , i.e., the graph diameter.

Hopping between the nodes in the discrete space of a network occurs through sinks (dark blue area in Figure 2) and sources (yellow area), where particles are allowed to hop to non-nearest nodes with a certain probability. Since the metaplexes that we study are undirected, the sinks also act as sources and vice-versa (see Supplementary Note 2). The evolution of the density of the diffusive particle among the nodes of the graph is controlled by the generalized diffusion equation [19]:

$$(2.4) \quad \frac{d\mathbf{u}(t)}{dt} = - \left(\sum_{d=1}^{d_{max}} c_d \Delta_d \right) \mathbf{u}(t), \quad \mathbf{u}(0) = \mathbf{u}_0,$$

where Δ_d is the d -path Laplacian operator of the graph transformed by the coefficients c_d . This operator is defined as follows. Let $C(V)$ denote the set of complex-valued functions in V . Let $f \in C(V)$, then [19]

$$(2.5) \quad \Delta_d f(v) = \sum_{w \in V, \text{dist}(v,w)=d} (f(v) - f(w)), \quad v \in V.$$

Notice that if we consider only $\text{dist}(v, w) = 1$ in the above definition, this operator becomes the graph Laplacian $\Delta_1 = L = K - A$, where K is a diagonal matrix of node degrees and A is the adjacency matrix of the graph. The transformation of the Δ_d operators through the coefficients c_d is aimed at tuning the hopping of the diffusive particle between nearest and non-nearest neighbors in the graph. For instance, let

$$(2.6) \quad \Delta_M f := \sum_{d=1}^{d_{max}} d^{-s} \Delta_d f,$$

designate the Mellin-transformed d -path Laplacians of the graph where d_{max} is the diameter of the graph.. Then, when $s \rightarrow \infty$ the transformed operator tends to

$\Delta_1 = L = K - A$. However, when s is relatively small the diffusive particle can hop not only to nearest neighbors but also to distant nodes with certain probability that decays with the shortest path distance separating the origin and destination of the particle. It was recently proved that in the one-dimensional lattice when $s \in (1, 3)$ there is a superdiffusive process on the graph [22]. The same happens for two-dimensional lattices when $s \in (2, 4)$ [23]. Other transforms, such as the exponential one, also known as the Laplace transform:

$$(2.7) \quad \Delta_e f := \sum_{d=1}^{d_{max}} e^{-ds} \Delta_d f,$$

can also be used in the generalized diffusion equation but they have been proved to show no superdiffusive processes on the graph [22].

In the analysis of the diffusion processes on metaplexes we will refer to the rate at which the diffusive particle reaches the steady state \bar{u} as $t \rightarrow \infty$. The rate of convergence of the diffusion on the metaplex is controlled by the standard deviation of the density, $\sigma(t) = \sqrt{\frac{1}{N-1} \sum_i \left(\int_{\Omega_i} u_i(t, \mathbf{x}_i) - \bar{u}_i \right)^2}$, where the summation is over all N nodes in V . In our examples the steady state \bar{u} is the uniform distribution on V .

3. Metaplexes: Structure and Dynamics. We have previously defined informally what a metaplex is. Here we present a formal definition of a metaplex and of a dynamical system on it. Let us start with the following.

DEFINITION 3.1. *A metaplex is a 4-tuple $\Upsilon = (V, E, \mathcal{I}, \omega)$, where (V, E) is a graph, $\omega = \{\Omega_j\}_{j=1}^k$ is a set of locally compact metric spaces Ω_j with Borel measures μ_j , and $\mathcal{I} : V \rightarrow \omega$.*

For instance, let us consider a simple metaplex in which (V, E) is a path graph, e.g., the path graph of 3 nodes with each node given by the unit disk $B(0, 1) \subset \mathbb{R}^2$. In this case $\omega = \{B(0, 1)\}$ and \mathcal{I} is constant. The resulting metaplex is illustrated in Figure 2. The endo-structure of this metaplex is given by the internal structure inside the unit disk, and its exo-structure is given by the connectivity of the three nodes in the form of a path. In the current work we focus only on metaplexes in which the internal structure of the nodes is continuous. That is, when ω is a set of open domains $\Omega_j \subset \mathbb{R}^n$, each endowed with the Lebesgue measure. Other scenarios in which the internal structure is a discrete space, not only a graph, should be considered in a separate analysis, and they will not be treated in the current work. Now, we are in condition to define a dynamical system on a metaplex.

DEFINITION 3.2. *A dynamical system on a metaplex $\Upsilon = (V, E, \mathcal{I}, \omega = \{\Omega_k\})$ is a tuple $(\mathcal{H}, \mathcal{T})$. Here $\mathcal{H} = \{H_v : L^2(\Omega_{\mathcal{I}(v)}, \mu_{\mathcal{I}(v)}) \rightarrow L^2(\Omega_{\mathcal{I}(v)}, \mu_{\mathcal{I}(v)})\}_{v \in V}$ is a family of operators such that the initial value problem $\partial_t u_v = H_v(u_v)$, $u_v|_{t=0} = u_0$, is well-posed, and $\mathcal{T} = \{T_{vw}\}_{(v,w) \in E}$ is a family of bounded operators $T_{vw} : L^2(\Omega_{\mathcal{I}(v)}, \mu_{\mathcal{I}(v)}) \rightarrow L^2(\Omega_{\mathcal{I}(w)}, \mu_{\mathcal{I}(w)})$.*

There are many possible dynamical systems that can be considered on a metaplex under the previous general definition. In the current work we focus only on the study of diffusive processes at the endo- and exo-structure of the metaplexes. In this scenario we consider a continuous diffusion equation inside the nodes where the evolution of the density of the diffusive particle is controlled by the fractional Laplacian operator

as described in [Section 2](#). At the exo-skeleton we consider a diffusive process in which the particle hops from a node to another as controlled by the d -path Laplacian of the graph also described in [Section 2](#). The in and out motion of the diffusive particle between nodes is carried out through the so-called *sources* and *sinks* inside the nodes. A source is a subdomain inside the node from which a diffusive particle can emerge to the interior of the node. A sink is another (not necessarily different) subdomain inside the node from which a diffusive particle can abandon the interior of the node towards another node in the metaplex.

In the simplest case, diffusive particles move between different nodes through such sinks and sources in the interior, corresponding to a coupled system of diffusion equations for the density $u_j(t, \mathbf{x})$ of particles in the node $v_j \in V$:

$$(3.1) \quad \begin{aligned} \partial_t u_j(t, \mathbf{x}) = \operatorname{div} J_j(u_j(t, \mathbf{x})) - \sum_{i: (v_j, v_i) \in E} \alpha_{ij}(\mathbf{x}) u_j(t, \mathbf{x}) \\ + \sum_{i: (v_i, v_j) \in E} \alpha_{ji}(\psi_{ji}^{-1}(\mathbf{x})) \det(\nabla \psi_{ji}^{-1}) u_i(t, \psi_{ji}^{-1}(\mathbf{x})), \end{aligned}$$

for $(t, \mathbf{x}) \in (0, \infty) \times \Omega_j$. Here J_j is the flux of particles, and $\operatorname{div} J_j$ is the generator of the diffusion process in Ω_j , for example $\operatorname{div} J_j = \Delta$ in the case of a normal diffusion, while $\operatorname{div} J_j = -(-\Delta)^s$ for the superdiffusive Lévy process. The edges $(v_i, v_j) \in E$ are realized by a map $\psi_{ji} : \Omega_j \rightarrow \Omega_i$ which specifies the jumps between domains, and the coefficients $\alpha_{ji}(\mathbf{x})$ are transition rates from Ω_i to Ω_j : Particles jump from \mathbf{x} to $\psi_{ji}(\mathbf{x})$ with amplitude $\alpha_{ij}(\mathbf{x})$ and from $\psi_{ji}(\mathbf{x})$ to \mathbf{x} with amplitude $\alpha_{ji}(\psi_{ji}^{-1}(\mathbf{x}))$. Physically, the system (3.1) arises for nodes which correspond to spatially distant domains.

For the system of diffusion equations (3.1), $H_{v_j} u_j = \operatorname{div} J_j(u_j)$, while T_{vw} correspond to the entries of the transition matrix of the network given by the functions α_{ij} .

Diffusion in a network may be studied from its generator, the graph Laplacian Δ_1 . A dynamical system in a metaplex is similarly described by an operator matrix \mathcal{D} . For the diffusion processes like (3.1) it takes the abstract form

$$(3.2) \quad \partial_t u = \mathcal{D} u.$$

\mathcal{D} is an $N \times N$ block operator matrix of unbounded operators on the product space $\bigoplus_{j=1}^N L^2(\Omega_j, \mu_j) = L^2(\Omega_1, \mu_1) \times \cdots \times L^2(\Omega_N, \mu_N)$, with N the number of nodes in V . In line with [Definition 3.2](#) we write $\mathcal{D} = H + T$, where

$$H = \begin{pmatrix} \operatorname{div} J_1 & 0 & 0 & \cdots & 0 \\ 0 & \operatorname{div} J_2 & 0 & \cdots & 0 \\ \vdots & 0 & \ddots & & \vdots \\ \vdots & \vdots & & \ddots & \vdots \\ 0 & 0 & \cdots & \cdots & \operatorname{div} J_N \end{pmatrix},$$

is given by the operators $H_{v_j} u_j = \operatorname{div} J_j(u_j)$ and

$$T = \begin{pmatrix} \alpha_{11} T_{11} & \alpha_{12} T_{12} & \cdots & \alpha_{1N} T_{1N} \\ \alpha_{21} T_{21} & \alpha_{22} T_{22} & \cdots & \alpha_{2N} T_{2N} \\ \vdots & \vdots & \ddots & \vdots \\ \alpha_{N1} T_{N1} & \alpha_{N2} T_{N2} & \cdots & \alpha_{NN} T_{NN} \end{pmatrix},$$

describes the network diffusion defined a \mathcal{T} . Provided the adjoint $T^* \begin{pmatrix} 1 \\ 1 \\ \vdots \\ 1 \end{pmatrix} = 0$,

particles are conserved. Here the T_{ij} are transition operators between Ω_i and Ω_j , as given by the sources and sinks, and α_{ij} are the transition probabilities.

For a network, spectral properties of the network Laplacian determine the long-time behavior of diffusion. Analogously, the long-time behavior of the linear diffusion equation (3.2) in the metaplex is determined by the spectral properties of \mathcal{D} [62]. While the spectrum of H is determined by the internal structure of the nodes, the spectrum of T combines the details of the location and strength of sinks, respectively sources, with the external network structure.

In addition to the coupling by sinks and sources as in (3.1), numerous other types of couplings can be considered within the framework of metaplexes. While their detailed analysis is beyond the scope of this paper, we mention two important examples.

The first example is a special case of (3.1), with all nodes of the same geometry $\Omega = \Omega_j$ for every j and local transitions $\psi_{ji} = \text{Id}$, where Id is the identity operator (matrix) of the appropriate dimension. In this case the density u may be interpreted as a vector valued function $u = (u_1, \dots, u_N) : [0, \infty) \times \Omega \rightarrow \mathbb{R}^N$, and the network encodes the dynamics of the “internal state” of the particle described by a vector in \mathbb{R}^N . In biology, such processes are of interest to describe the diffusion of complex organisms [54, 18, 17].

In complex systems such as road systems or the transport of chemicals between cells, the coupling between the nodes occurs through the boundary $\partial\Omega_j$, not through internal sinks and sources. Every edge $(v_i, v_j) \in E$ is physically realized by open entrances and exits $\Gamma_{ij} \subset \partial\Omega_i$ and $\Gamma_{ji} \subset \partial\Omega_j$, together with a homeomorphism $\phi_{ij} : \Gamma_{ij} \rightarrow \Gamma_{ji}$ identifying points between them. We define $\Gamma_{i0} = \partial\Omega \setminus \bigcup_j \Gamma_{ij}$. If there is an edge between Ω_i and Ω_j , particles leave Ω_i through Γ_{ij} and arrive at Γ_{ji} in Ω_j .

The resulting system of diffusion equations is coupled through the boundary conditions, with a Kirchhoff’s law: For $\mathbf{x} \in \bigcup_i \Gamma_{ji}$

$$u_j(t, \mathbf{x}) = \sum_{i: \mathbf{x} \in \Gamma_{ji}} \alpha_{ji} \det(\nabla_{\partial\Omega} \phi_{ji}) u_i(t, \phi_{ji}(\mathbf{x})) ,$$

$$J(u_j(t, \mathbf{x})) \cdot \nu_j(\mathbf{x}) = - \sum_{i: \mathbf{x} \in \Gamma_{ji}} \alpha_{ji} \det(\nabla_{\partial\Omega} \phi_{ji}) J(u_i(t, \phi_{ji}(\mathbf{x}))) \cdot \nu_i(\phi_{ji}(\mathbf{x})) ,$$

where ν_j is the exterior unit normal vector. The number of particles is preserved if the transition probabilities satisfy $\sum_i \alpha_{ji} = 1$ for every j .

4. Operators and spectra for metaplexes.

4.1. Variation of eigenvalues with fractional exponent and spatial scale.

Note that $H = \bigoplus_{j=1}^N H_j = \bigoplus_{j=1}^N \text{div} J_j$ is a block diagonal operator matrix acting on $L^2(\Omega_1) \times \dots \times L^2(\Omega_N)$. A basis of eigenfunctions of H is constructed from bases $\{u_{j,k}\}_k$ of eigenfunctions of $\text{div} J_j$ in Ω_j and it is given by $\{u_{j,k} e_j\}_{j,k}$ where the subscripts denotes the k -th eigenfunction in the domain Ω_j . Here e_j denotes the j -th standard unit vector in \mathbb{R}^N .

If $H_j = -(-\Delta)^{s_{nod}}$ is the fractional Laplacian in Ω_j with Neumann boundary conditions, the eigenvalues of H_j are homogeneous functions of the spatial scale, i.e., if the spatial variable is scaled, then also the function, $f(\alpha x) = \alpha^p x$, where p is the degree of homogeneity. More precisely, the bilinear form of H_j is homogeneous under scaling $\Omega_j \mapsto \Lambda \Omega_j$, $\Lambda > 0$. For instance, if $\Omega_j = B(0, 5)$ is a ball of radius 5, then the scaling of the domain can be interpreted as $\Lambda \Omega_j = B(0, \Lambda 5)$.

From their characterization in terms of a Rayleigh quotient, the eigenvalues in $\Lambda \Omega_j$ are given by $\{\Lambda^{-2s_{nod}} \lambda_{j,k}\}_{k=1}^\infty$, if $\{\lambda_{j,k}\}_{k=1}^\infty$ are the eigenvalues of H_j in Ω [13]. Only the lowest eigenvalue $\lambda_{j,1} = 0$ is fixed under this scaling.

We see that for small domains, $\Lambda \rightarrow 0$, the spectral gap $\lambda_{j,2} - \lambda_{j,1}$ in the node Ω_j increases with s_{nod} , and therefore Brownian motion in the nodes gives the fastest convergence to equilibrium. For large domains, $\Lambda \rightarrow \infty$, the spectral gap $\lambda_{j,2} - \lambda_{j,1}$ in the nodes Ω_j decreases with s_{nod} , and therefore the long jumps of the fractional diffusion lead to faster equilibration than Brownian motion inside each node.

In a further section (see Section 6) we will illustrate computationally these findings.

4.2. Weakly and strongly interacting limits. The spectral properties of $\mathcal{D}_\varepsilon = H + \varepsilon T$ are most easily understood in the limit $\varepsilon \rightarrow 0$ of weak network interactions between the nodes, respectively the strong network interactions for $\varepsilon \rightarrow \infty$. In the former case, a particle is trapped for a long time inside the domain in which it was initially placed. The time scale of the slow global equilibration is determined by T . In the latter case, the transient dynamics is governed by the dynamics of the network and geometry of the sinks and sources, i.e. T , but the dynamics H inside the nodes determines the long-time approach to equilibrium.

From standard perturbation theory, for general, symmetric interactions T the stationary states corresponding to $\lambda_{j,1} = 0$, $j \in \{1, \dots, N\}$, split into eigenvalues $\varepsilon \tilde{\lambda}_k + o(\varepsilon)$ according to the eigenvalues $\tilde{\lambda}$ of T restricted to the kernel of H . The kernel of H is spanned by the constant functions 1 in Ω_j , $j = 1, \dots, N$. Hence, $(T|_{\ker H})_{ij} = \frac{1}{\sqrt{|\Omega_i||\Omega_j|}} \int_{\Omega_j} \alpha_{ij} T_{ij} 1 \, dx$, $i, j = 1, \dots, N$, is given by an effective graph Laplacian for the metaplex, in which the internal structure has been integrated out. The eigenvalues $\tilde{\lambda}_k$ of this matrix determine the spectral gap $\varepsilon(\tilde{\lambda}_2 - \tilde{\lambda}_1)$ in terms of the spectral gap of the effective graph Laplacian $T|_{\ker H}$, independent of H . Higher eigenvalues will depend on the location of the sources and sinks and the eigenfunctions of H_j .

Multiple eigenvalues arise, in particular, when several of the H_j coincide. In this case the eigenvalues are determined by the restriction T_r of T to the subnetwork of those nodes where the internal diffusion has the eigenvalue $\lambda_{j,k}$.

Higher eigenvalues depend on the location of the sources and sinks. The spectral gap of the network is $\varepsilon \lambda_2$, and thus independent of the diffusion process H .

Local equilibration within the nodes, however, happens on faster time scales, with little effect of the coupling. For small ε , the gap between the higher bands $\lambda_{j,k} + \varepsilon \lambda_n^r$ to the equilibrium is determined by the diffusion H , up to terms of order ε , where $\{\lambda_n^r\}$ are the eigenvalues of T_r .

The case where $T_{ij} = \text{Id}$ is discussed in the Supplementary Material (Note 3). For general T_{ij} the spectrum of the network interaction operator T will be considered elsewhere.

4.3. Numerical results of the spectral properties. We illustrate the spectral gap of \mathcal{D}_ε for a linear network of 11 unit disks $\Omega = \Omega_j = B(0, 1) \subset \mathbb{R}^2$. The

lowest 10 nonzero eigenvalues are considered as a function of ε , the coupling operator T and the diffusion H . We choose the generator H_j of the diffusion process inside Ω_j as a fractional Laplacian $-(-\Delta)^{s_{nod}}$ with Lévy exponent s_{nod} and approximate it by finite elements on quasi-uniform spatial meshes. See Figure 6 below for a plot of the mesh and [24] for the approximation of the fractional Laplacian.

The network coupling T_{ij} is taken to be a d -path Laplacian (2.7) with hopping between Ω_i and Ω_j proportional to an exponential $2^{-s_{net}|i-j|}$.

As H is unbounded the eigenvalues of its discretization extend over several orders of magnitude, while the spectral gap is tiny. To resolve it, the discretization of the mesh h needs to be small compared to the strength of the coupling, and standard Matlab routines do not identify the bounded branches of eigenvalues obtained in Subsection 4.2 for large ε . Discretization errors significantly increase as $s_{nod} \rightarrow 0$ because the smoothness of the solutions in Ω decreases.

Figure 3 indicates the complications inherent in approximating the spectrum of a large system of differential operators. The lowest 10 nonzero eigenvalues of \mathcal{D}_ε are depicted for the exponential coupling as a function of the coupling strength $\varepsilon \in [2^{-10}, 2^{10}]$ for meshes of 347 and 1325 degrees of freedom, $s_{net} = 0.8$, $s_{nod} = 0.4$. We consider a prototypical metaplex coupling as depicted in Figure 2 for $\alpha_{ij} = 10$. While results agree for large coupling strengths, the spectral gap is significantly smaller for the finer mesh at small coupling. Nevertheless, the qualitative behavior from Subsection 4.2 is recovered: the gap increases linearly for small ε , and for large ε it converges to the lowest eigenvalue of H .

Figure 4 connects the theory of Subsection 4.2 with the numerical results from Section 6 and evidences the effect of the geometry of the nodes on the dynamics of the network. In the case of the small nodes (Figure 4 left) when the coupling is weak, the dynamics of the network is dominated by the diffusion process inside the nodes and we have almost no hopping between domains. As we increase the coupling strength, for $s_{nod} = 0.8$ the spectral gap is bigger than that for $s_{nod} = 0.2$ in agreement with Subsection 4.1. Similar to the case of multiplex networks, the first non-zero eigenvalue of \mathcal{D}_ε is related to the equilibration time in the whole networks, i.e., $t = \lambda_2^{-1}$ [61]. From Figure 4 (left) the equilibration time for the case $s_{nod} = 0.2$ is much longer than for the normal diffusion case inside the nodes. In a further section of this work (see Section 6) we obtain computational results that confirm the current findings.

In the case of big nodes (Figure 4 right) the spectral gap decreases as we increase the parameter s_{nod} . This means that, opposite to the small node case, a metaplex with superdiffusion inside the nodes ($s_{nod} = 0.2$) reaches the equilibrium faster than for internal Brownian motion.

5. Analysis of diffusion in metaplexes. In this section we indicate how PDE techniques allow an analysis of the time-dependent diffusion introduced in Section 3 in a metaplex of bounded domains $\omega = \{\Omega_j \subset \mathbb{R}^n\}_{j=1}^k$, as illustrated in Figure 2. We compare the interaction of diffusion, respectively superdiffusion, in the nodes with either short or long range coupling in the external network. While for general complex networks the connectivity and large scale geometry of the network will crucially influence the dynamics, here we focus on simple linear metaplexes $V = Q = \{\dots, -2, -1, 0, 1, 2, \dots\}$ and short times.

More precisely, we assume that the diffusion process in each node Ω_j is governed by either a fractional Laplacian $H_j = -(-\Delta)^{s_{nod}}$ or a self-adjoint elliptic differential operator of second order like the Laplacian, $H_j u_j = \text{div}(a \nabla u_j)$, $a \in C^\infty(\bar{\Omega}_j)$, with Neumann boundary conditions. The network coupling T_{ij} consists of disjoint sinks

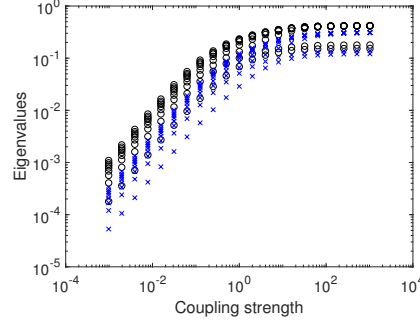


FIG. 3. Comparison of eigenvalues for the case of different discretizations h of the mesh: a coarse mesh (347 degrees of freedom) (\circ) and a finer mesh (1325 degrees of freedom) (\times). Here $s_{net} = 0.8$ and $s_{nod} = 0.4$ and we consider different coupling points.

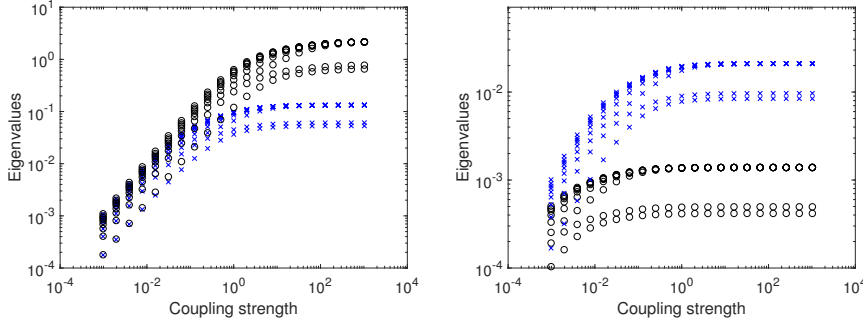


FIG. 4. Eigenvalues for small (left) and big (right) nodes. In both cases $s_{net} = 0.8$ with $s_{nod} = 0.2$ (crosses) and $s_{nod} = 0.8$ (circles).

and sources, as in Figure 2. The amplitude is chosen according to the d -path Laplacian (2.6), (2.7), with hopping between Ω_v and Ω_w proportional to $\text{dist}(v, w)^{-s_{net}}$ (long range coupling), respectively $2^{-s_{net}\text{dist}(v, w)}$ (short range coupling).

When we consider a metaplex we are dealing with the endo-dynamics occurring inside the nodes and the exo-dynamics occurring between them. Inside each node Ω_j the solution $e^{tH_j}u_{j,0}$ to the diffusion equation for H_j with initial condition $u(t=0) = u_{j,0}$ is an integral operator $(e^{tH_j}u_0)(t, \mathbf{x}) = \int_{\Omega} K_{H_j}(t, \mathbf{x}, \mathbf{y})u_0(\mathbf{y}) d\mathbf{y}$. The integral kernel K_{H_j} describes the evolution of a Dirac point mass in \mathbf{y} at time $t = 0$. For ordinary diffusion away from the boundary $\partial\Omega_j$ it satisfies the Gaussian estimate

$$(5.1) \quad |K_{H_j}(t, \mathbf{x}, \mathbf{y})| \leq Ct^{-n/2}e^{-C\frac{|\mathbf{x}-\mathbf{y}|^2}{t}}$$

for some $C > 0$, analogous to the explicit solution formula for the diffusion equation on \mathbb{R}^n [53]. Similar bounds are known for ordinary diffusion on metric measure spaces Ω_j [32]. Fractional diffusion, on the other hand, exhibits slow algebraic decay in the form of a Poisson estimate

$$(5.2) \quad |K_{H_j}(t, \mathbf{x}, \mathbf{y})| \leq Ct \left(|\mathbf{x} - \mathbf{y}| + t^{1/(2s_{nod})} \right)^{-n-2s_{nod}}$$

away from $\partial\Omega_j$ [28]. In a convex domain the estimate is sharp for short times, and it allows us to estimate the diffusion between nodes across the network.

Consider the linear network in [Figure 2](#), with an initially uniform density localized in Ω_1 . From [Equation \(3.1\)](#) we calculate the change of the total density in node j :

$$(5.3) \quad \partial_t \Big|_{t=0} \int_{\Omega_j} u_j(t, \mathbf{x}) \, d\mathbf{x} = -\frac{\delta_{j1}}{|\Omega_1|} \sum_i \int_{\Omega_j} \alpha_{ij}(\mathbf{x}) d\mathbf{x} + \frac{1}{|\Omega_1|} \int_{\Omega_j} \alpha_{j1}(\psi_{j1}^{-1}(\mathbf{x}) \det(\nabla \psi_{j1}^{-1})) \, d\mathbf{x}.$$

So, initially particles hop from node 1 to node j according to the transition probabilities α_{ij} of the network, from \mathbf{x} to $\psi_{j1}(\mathbf{x})$. From Duhamel's formula for the solution of the inhomogeneous diffusion equation, they then evolve inside Ω_j according to K_{H_j} before jumping back to node 1, or further to a different node k . Both processes only enter into the next, quadratic term of the Taylor expansion in t . These formal arguments are made rigorous in terms of an asymptotic expansion for $t \rightarrow 0$ of the heat kernel $K_{\mathcal{D}}$ for the network of interacting domains, see e.g., [\[45\]](#).

Compared to nodes without internal structure, hopping to node k is reduced by the rate $K_{H_j}(\tau, \psi_{j1}(\mathbf{x}), \mathbf{y})$ of diffusing from $\psi_{j1}(\mathbf{x})$ to a point \mathbf{y} in the region of the sink to node k within time τ . The internal diffusion thus always slows down the network dynamics if sources and sinks are disjoint.

The exit time $\tau_{source, sink}^j$ taken to get from source to sink is well studied both for normal and fractional diffusion [\[2\]](#). It satisfies a (fractional) Fokker-Planck equation and satisfies the estimate [\(5.1\)](#), respectively [\(5.2\)](#), for short times. For long times, $\tau_{source, sink}^j$ decays exponentially fast in time.

For short times, the dependence on the internal diffusion H_j , the geometry of Ω_j , and the location of sinks and sources are well described by [\(5.1\)](#) and [Equation \(5.2\)](#). For sources and sinks which are far apart, in the case of normal diffusion [Equation \(5.1\)](#) shows a faster than exponential suppression of the transition rate due to the internal structure. Fractional diffusion suppresses the transition rate algebraically in the distance between sink and source, according to [Equation \(5.2\)](#). The smaller s_{nod} , the faster the equilibration and the smaller the suppression in Ω_j .

Similarly if T_{ij} is nonzero only for $|i - j| \leq 1$, hopping to next j -th nearest neighbors is suppressed j times by the internal diffusion. Starting from an initial density localized in node 1, the total density in node j will be exponentially small, $\int_{\Omega_j} u_j(t, \mathbf{x}) \, d\mathbf{x} \leq C e^{-C|j-1|}$ for some $C = C(t) > 0$ depending on the endo-structure.

6. Numerical analysis of diffusion in metaplexes. This section investigates the influence of the internal structure of the nodes on the global metaplex dynamics, using numerical experiments for the toy example of a linear metaplex. For the localized coupling T_{ij} in a given area ([Figure 5](#)) we show the rich dependence on the internal structure in a metaplex such as the geometry of the nodes and the nature of the coupling, and put the results, which we obtained in certain limits, into a wider perspective. For example, a superdiffusive process in the nodes may *slow down* equilibration in the metaplex, see Experiment 1. On the other hand, the network diffusion dominates the qualitative global behavior: In [Subsection 6.3.1](#) we show that network superdiffusion due to long range hopping survives independently of the internal structure. This section illustrates the rich phenomena which arise from the interplay of the exo- and endo-structures of the metaplex. See Supplementary Information for numerical and analytical results for the case $T_{ij} = \text{Id}$. The conclusions are not restricted to the linear metaplex, but will be studied in the subsequent section in some real-world examples.

6.1. Set up of numerical experiments. Here we analyze a simple metaplex consisting of 51 identical circular domains $\Omega = \Omega_j \subset \mathbb{R}^2$ connected in the form of a

linear chain, i.e., a path graph. The nodes are labelled in consecutive order starting by one. Starting from a uniform distribution in node 1, we study the evolution of the density in the nodes depending on the network and the internal diffusion processes, the size of the nodes and the strength and nature of the coupling between the nodes.

Two different sizes of nodes are considered, $\Omega_s = B(0, 1)$, $\Omega_b = B(0, 100)$. These different sizes will also be used when we move to the analysis of real-world metaplexes. The diffusion equation (3.1) inside each node with Lévy exponent s_{nod} is approximated by finite elements in space on a quasi-uniform spatial mesh with 347 degrees of freedom. See Figure 6 for a plot of the mesh and [24] for the numerical approximation of the fractional Laplacian. For the time discretization we use a backward Euler method in time with a sufficiently small, fixed time step $dt = 0.01$.

Unless stated otherwise, the network coupling between nodes (i, j) is taken to be of short range, according to the Laplace-transformed d -path Laplacian (2.7). The coupling strength between nodes (i, j) is thus proportional to $2^{-s_{net}|i-j|}$ for different exponents s_{net} .

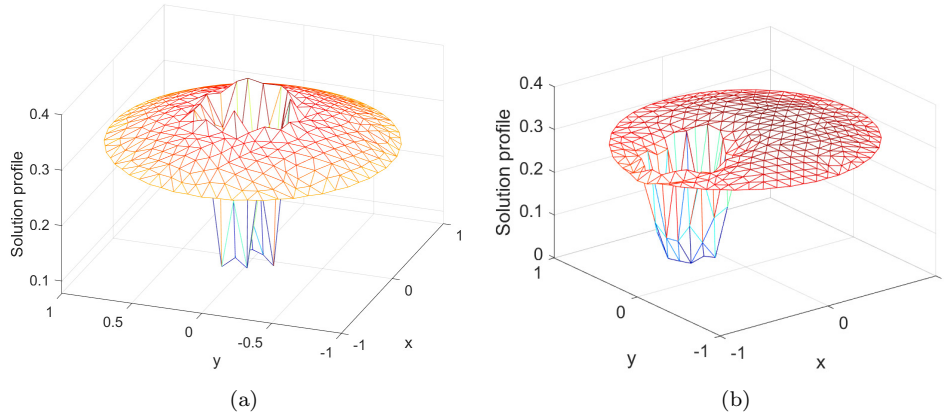


FIG. 5. Density profile for different coupling points between nodes.

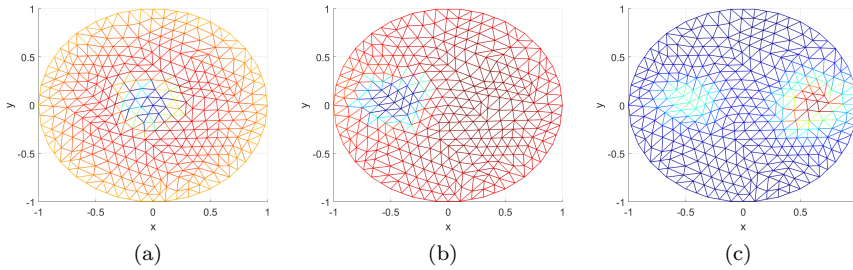


FIG. 6. Mesh inside the nodes for the different coupling areas in experiment 1 (a) and experiment 2 (b, c).

6.2. Experiment 1: Central coupling region. For different values of the network exponent $s_{net} = 0.4, 0.8$, we compare close to normal diffusion (Lévy exponent $s_{nod} = 0.8$) to superdiffusion ($s_{nod} = 0.2$) inside a metaplex of small nodes Ω_s . In

this experiment we consider that the nodes of the metaplex are connected by means of a central region of the node, as depicted in Figure 5a, which acts at the same time as a sinks and as a source. See Supplementary Material (Note 2) for a more detailed description of sink and sources. The coupling strength is fixed to be $\alpha = 10$.

Figure 7 shows the time at which the density in node 1 reaches the equilibrium given by $|\int_{\Omega_1} u_1(t, \mathbf{x}) d\mathbf{x} - \frac{1}{N} \int_{\Omega_1} u_0(\mathbf{x}) d\mathbf{x}|$, where $u(t, \mathbf{x})$ is the density in the node at a given time t and $u_0(\mathbf{x})$ is the initial density in the metaplex. The figure illustrates the strong effect of the dynamics inside the nodes on the diffusion process, even though the networks dynamics dominates. We see that superdiffusion inside each node slows down the diffusion in the network: Due to the nature of the Lévy process, particles quickly diffuse far away from the sink. As they take time to return and hop to the next node, diffusion between nodes in the whole network is slowed down. In Subsection 6.3 we discuss how the size of the nodes affects this behavior.

The spatial localization of the sink and sources decreases the total strength of the coupling, resulting in a slower equilibration of the densities in the node compared to a uniform coupling discussed in the Supplementary Material (Note 3). Changing the strength of a sufficiently strong localized coupling does not affect this behavior much, as the equilibration time saturates: independent of the coupling strength, particles which are located away from the sink cannot hop to a neighboring node.

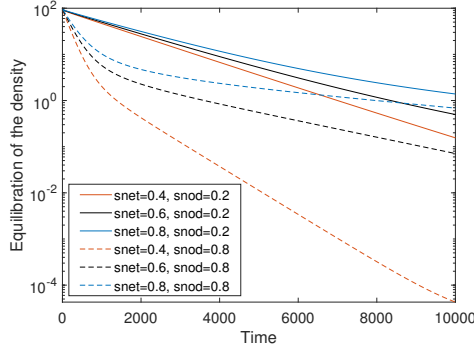


FIG. 7. Density equilibration in node 1 for central coupling region.

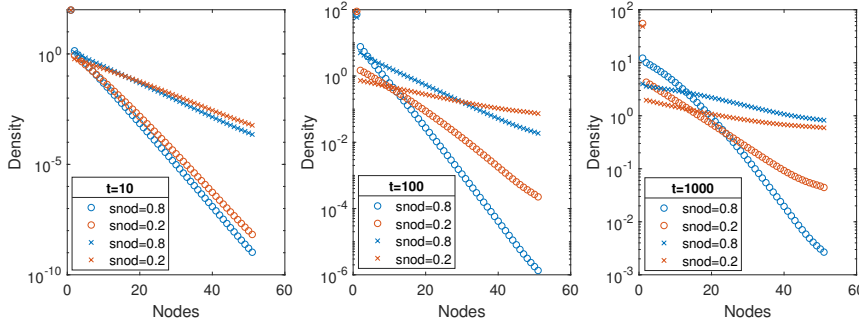


FIG. 8. Density distribution for central coupling region, $s_{net} = 0.8$ (\circ), resp. 0.4 (\times).

In [Figure 8](#) we show the evolution in time of the total density $\int_{\Omega_j} u_j(t, \mathbf{x}) d\mathbf{x}$ in each node Ω_j . While superdiffusion inside the nodes has only limited effect on the equilibration of the densities in the network, it speeds up hopping to distant nodes. From [Figure 8](#) we observe that, when the network dynamics is dominated by superdiffusion ($s_{net} = 0.4$), only for short times the superdiffusion inside the nodes (red crosses) overtakes normal diffusion, while for longer times the equilibrium is attained faster for $s_{nod} = 0.8$.

6.3. Experiment 2: Distant coupling regions. To study the effect of the geometry of the coupling and the node on the global dynamical process, we replace the central coupling from [Subsection 6.2](#) by a prototypical metaplex coupling as depicted in [Figure 2](#): For the odd nodes the coupling region is located as in [Figure 5b](#), while for even nodes the coupling region is on the opposite side. Similar to the central coupling, the coupling regions act as sink and as sources at the same time. The coupling areas in both domains are equal, therefore, in the case of Ω_b , the areas are more localized and distant.

For the network dynamics, we consider the short range coupling from Experiment 1 given by the Laplace-transformed d -path Laplacian (2.7), with coupling between nodes (i, j) proportional to $2^{-s_{net}|i-j|}$, $s_{net} = 0.4, 0.8$. The coupling strength is fixed to be $\alpha = 10$ for Ω_s and $\alpha = 100$ for Ω_b . In [Subsection 6.3.1](#) we compare the resulting dynamics to a long range coupling proportional to $|i - j|^{-s_{net}}$, with the Mellin-transformed d -path Laplacian (2.6).

In the current experiment, the distance between the sinks and sources also leads to a delay; particles appear in the node and have to diffuse to find the sink to hop to another node. Coupled with the exo-dynamics, the delay leads to small density oscillations between neighboring nodes. For clearer illustration in [Figures 10, 11, 13](#) and [14](#) we only consider the odd nodes of the metaplex.

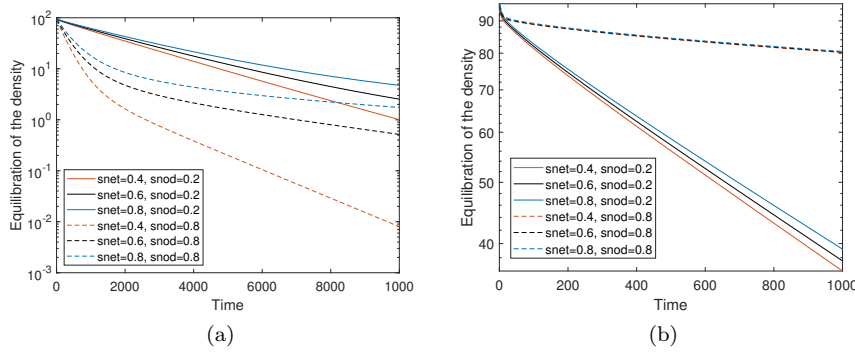


FIG. 9. Density equilibration in node 1 for disjoint sinks and sources (a) Ω_s (b) Ω_b .

[Figure 9a](#) shows the deviation of the density in node 1 from equilibrium, corresponding to [Figure 7](#) in Experiment 1. Similar to Experiment 1, superdiffusion inside the small nodes Ω_s slows down equilibration. However, the evolution in time of the total density $\int_{\Omega_j} u_j(t, \mathbf{x}) d\mathbf{x}$ in nodes Ω_i is depicted in [Figure 10](#), at times $t = 10, 100, 1000$. One observes that superdiffusion in the nodes allows particles to reach distant nodes more efficiently than approximately normal diffusion $s_{nod} = 0.8$. This confirms the interpretation in [Section 4](#). The case $s_{net} = 0.4$ in [Figure 10](#) exhibits

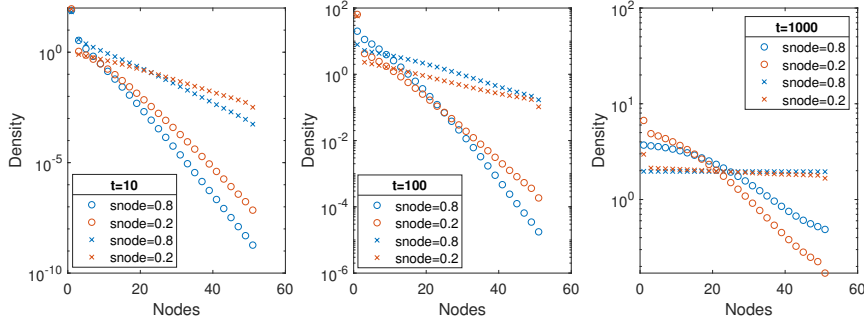


FIG. 10. Density distribution for small nodes Ω_s , $s_{net} = 0.8$ (\circ), resp. 0.4 (\times).

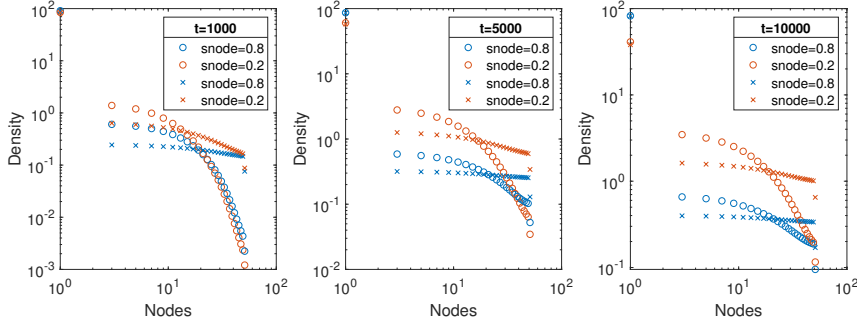


FIG. 11. Density distribution for big nodes Ω_b , $s_{net} = 0.8$ (\circ), resp. 0.4 (\times).

similar dynamics as in Experiment 1, where $s_{nod} = 0.8$ equilibrates the metaplex's density faster on long time scales.

We conclude that particles undergoing approximately normal diffusion ($s_{nod} = 0.8$) are slower, but more precise. Superdiffusing particles ($s_{nod} = 0.2$) explore the metaplex faster, but take more time to equilibrate the density across the whole metaplex. Similar observations have been made in [44], where the targeting efficiency of *E. coli* bacteria was studied in simulations. They observed that bacteria with higher motility, following a superdiffusion process, found targets faster, but were also at risk of moving rapidly away from the target due to the nature of their Lévy walk. Individuals with lower motility were slower but more precise.

The following figures compare these conclusions to those obtained for a network of big nodes Ω_b .

In Figure 9b we observe that superdiffusion inside big nodes speeds up the equilibration of the densities considerably: For $s_{nod} = 0.2$ particles require a much smaller time to reach their distant target, the sink, than for $s_{nod} = 0.8$. This is in agreement with the discussion in Subsection 4.1.

In Figure 11 we plot the density as a function of the node, in a log-log plot at times $t = 1000, 5000, 10000$. Note that because of the large distance between sources and sinks for nodes Ω_b , the time scale to approach equilibrium increases significantly. We observe that superdiffusion inside the nodes accelerates the equilibration over the

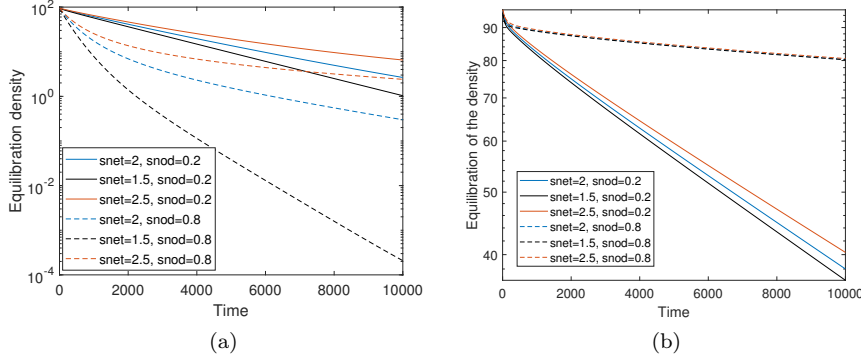


FIG. 12. *Density equilibration in node 1 for the Mellin-transformed d -path Laplacian for Ω_s (a) and Ω_b (b).*

whole metaplex in all cases, unlike for the small nodes Ω_s (Figure 10). For $s_{net} = 0.4$ in Figure 11 we observe the accelerated diffusion clearly, with a density distribution which is far from a Gaussian parabola in the log-log plot.

6.3.1. Metaplex superdiffusion. From the discussion of Experiments 1 and 2 so far, we conclude that for the short ranged network diffusion (2.7), proportional to $2^{-s_{net}|i-j|}$, superdiffusion in the nodes can accelerate the equilibration in the metaplex, but it cannot lead to global superdiffusion. This is in line with the discussion in Section 5. We now consider a long ranged network coupling proportional to $|i-j|^{-s_{net}}$, given by the Mellin-transformed d -path Laplacian (2.6) for $s_{net} = 1.5, 2, 2.5$ and 4.

In the case of this linear metaplex we count with the advantage that previous analytic results exists for the diffusion on its exo-skeleton using the d -path Laplacians [19]. In this case it was proved analytically that the use of the Mellin transform may produce superdiffusive regime in an infinite linear chain of nodes for $s_{net} \in (1, 3)$.

As in Figure 11, Figure 13 plots the density at times $t = 10, 100, 1000, 10000$ as a function of the node of the network in a log-log plot. The linear decay of the density and the peaked behaviour at node 1 indicate superdiffusion irrespective of the internal dynamics. Because of the strong network diffusion, for the big nodes Ω_b the structure of the nodes proves irrelevant to the metaplex dynamics.

In Figure 14 we exhibit the absence of superdiffusion for large Mellin exponent $s_{net} = 4$ and $s_{nod} = 0.8$: The density distribution recovers a Gaussian shape, characteristic of normal diffusion, as is clearly visible for longer times. Note that for the illustration of the Gaussian shape we have symmetrically reflected the network with respect to the y -axis.

Finally, Figure 12 shows the equilibration of the density in node 1 with time. It confirms the interplay of the nodal diffusion process and the size of the node, as observed for the short ranged network diffusion above in Figure 9.

In closing, after all the analyses carried out in this section we can conclude that for the path graph \mathcal{Q} and for T_{ij} given by the d -path Laplacian (2.7), there exists $C > 0$ such that $\int_{\Omega_j} u_j(t, x) dx \leq Ce^{-C|j-1|}$ for $j \in \mathcal{Q}$. In particular, superdiffusion is not possible for the considered internal diffusion $\{H_k\}_k$.

In the case of the Mellin-transformed d -Laplacian (2.6), the numerical results indicate that superdiffusion in the network may persist even for nodes with distant

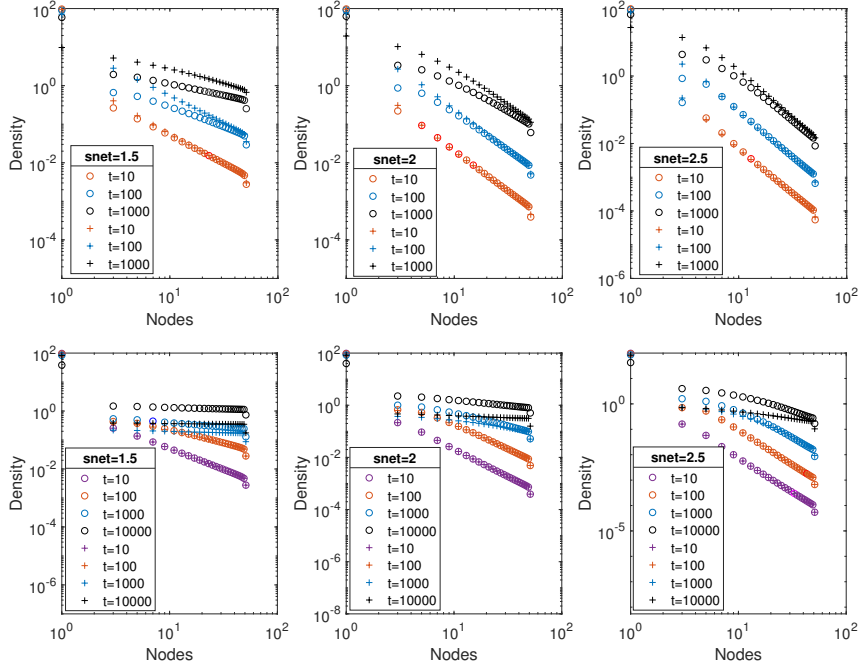


FIG. 13. *Density distribution for long ranged network coupling, $s_{nod} = 0.2$ (\circ) and $s_{nod} = 0.8$ ($+$). Top panel: Ω_s . Bottom panel: Ω_b*

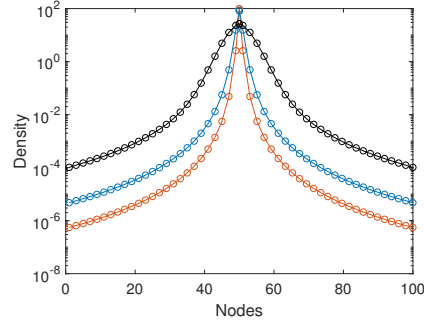


FIG. 14. *Gaussian shape of density distribution for $s_{net} = 4$ and $s_{nod} = 0.8$ at $t = 10$ (red), $t = 100$ (blue) and $t = 1000$ (black).*

sinks and sources. While in general the range of Mellin exponents s_{net} which allow superdiffusion may shrink, for certain experiments in the linear network $V = \mathcal{Q}$ we numerically recover superdiffusion for $s_{net} \in (1, 3)$, as in absence of internal structure [22].

7. Real world metaplexes. In this section we study the diffusion in two real-world metaplexes of very distinctive type. The first, a landscape metaplex representing a fragmented forest from the south of Madagascar which shares some of the large-world properties of the linear metaplex in Section 6. A metaplex representing the cortical region of a macaque, used as a second example, illustrates the dominance of

the endo-dynamics in an ultra small-world network.

Here we focus on the diffusive processes on both systems. The analogies between brain and ecological anomalous diffusion seem to be more than casual. Costa et al. [12] have coined the term “foraging brain” to refer to these similarities, and the connection between animal foraging and cognitive foraging has been considered by Hills [33] on an evolutionary basis.

In the following subsections we consider either small Ω_s or big Ω_b disks for all the nodes in the metaplex exactly as defined for the toy model. The goal of this is to analyze whether the size of the nodes have some influence on the global dynamics of the metaplex. Thus, we can consider that Ω_s and Ω_b are average sizes of the regions in the corresponding metaplex, such average is either relatively small or big. The coupling strength is given by $\alpha = 10$ for the small nodes Ω_s , and $\alpha = 100$ for the big nodes Ω_b . The nature of the coupling, as for the toy model in Section 6, is considered to be long ranged, proportional to $\text{dist}(i, j)^{-s_{net}}$ according to the Mellin transformed d -path Laplacian (2.6). The results for the short range coupling can be found in the Supplementary Material (Note 4).

For the landscape metaplex we discretize each node using a finite element method with 95 degrees of freedom, while for the metaplex of the cortical regions of a macaque we use a mesh of 347 degrees of freedom

The study of real-world metaplexes imposes some limits to the models in use which were not needed for the idealistic toy model studied before. The first is that the consideration of a unique source and sink at the centre of each node seems unreasonable. For both cases, the landscape and the visual cortex, we consider spatial regions which can be connected to each other by disjoint sources and sinks as in Figure 5b.

7.1. Landscape metaplex. The first example considered represents a landscape in the south of Madagascar that has been fragmented into 183 patches, corresponding to the nodes of a metaplex, as a result of agricultural activity [6]. These patches are connected by 529 narrow corridors that creates the exo-structure of the metaplex. Such patches are vital for the survival of the ecosystem because they are now the main habitat for the *Lemur catta*, who plays a fundamental role as a major seeds propagator in this environment [5, 21].

Here we assume that all the patches have the same geometry. The network has relatively low edge density – number of edges divided by the maximum possible number of edges – $\delta \approx 0.032$ with about 45% of nodes with degrees 2 and 3, and only two nodes with degree 16. The average separation between two patches in terms of the shortest path distance is approximately 11.88 with at least one pair of patches separated at $d_{max} = 32$. The average degree of the patches is approximately 5.78 and the maximum number of nearest neighbors that a patch has is 16.

Also, we can observe that most of the hubs – high degree nodes – are clumped together in a certain region of the landscape (see Figure 15a), while the low degree nodes are relatively spread across the landscape. Consequently, we have initialized the diffusive process by placing the initial condition either into a randomly selected hub or into a randomly selected low-degree node.

The next experiment allows us to investigate whether the degree of the node at which the diffusion starts makes an important influence on the global metaplex diffusion.

In Figure 16 we plot the density of the diffusive particle as a function of the shortest path distance from the initial condition when the diffusion starts at a low

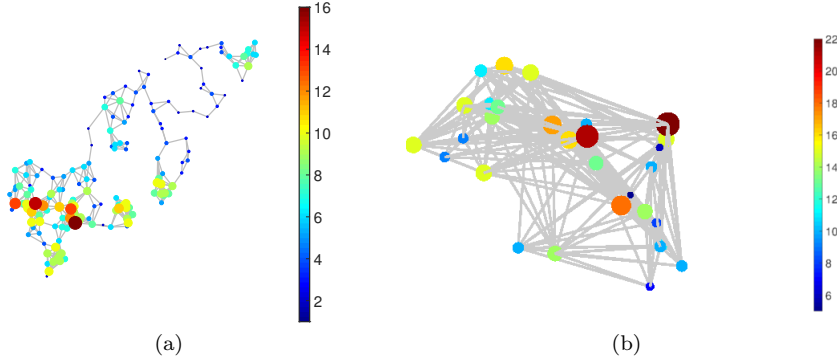


FIG. 15. Illustration of the exo-skeleton of a landscape (a) and a macaque metaplex (b) studied here. The nodes are drawn with size and color proportional to their degrees.

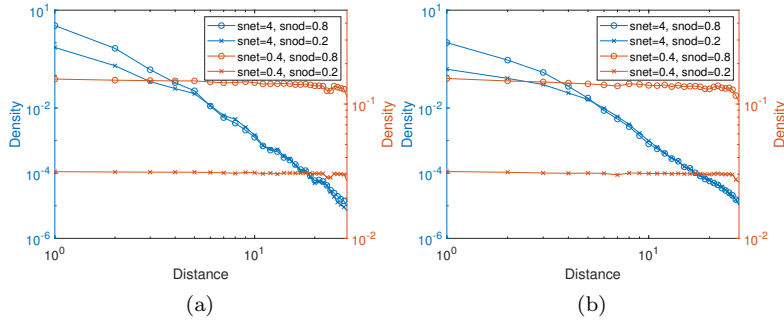


FIG. 16. Density as a function of distance for disjoint coupling point at $t = 100$. (a) Low connectivity nodes. (b) High connectivity nodes.

(Figure 16a) or at a high (Figure 16b) degree node. Here we averaged all the densities for nodes at exactly the same shortest path distance from the initial condition where three different nodes with high (resp. low) connectivity were chosen to initialize the process. We observe that there are no significant differences between Figure 16a and Figure 16b. Only when $s_{net} = 4$ there are some differences between the process initiated at low and at high degree nodes. In this particular case, it seems that when the process starts at a low degree node the density at nodes close to the initial condition shares more concentration than those more distant from it. This localization effect can be the consequence not of the degree of the node but of the relative geographic isolation that such nodes can display in this landscape. That is, one low-degree node is essentially surrounded by other low-degree nodes (see Figure 15a). However, in all the other cases it is important to remark that the profiles of the density at different distances from the initial conditions are almost exactly the same for processes starting at low or high degree nodes. Consequently, we conclude that in this metaplex the place at which the diffusion is initiated is not relevant for the evolution of the global process. Therefore, in the rest of this section we discuss the results for the process started from low-degree nodes.

We now explore the influence of the geometry of the nodes. In Figure 17 we plot the change of the density for nodes at different shortest path distances from the initial condition, for a small (Figure 17a) and big node (Figure 17b) using the same

value of $s_{net} = 0.4$. The first clear observation from these plots is the following. When the nodes are small, superdiffusion inside the nodes slows down the rate to the equilibration of the diffusion in the metaplex (notice that crosses are over the circles in Figure 17a). However, when the nodes are big, the reverse occurs, and relatively high values of $s_{nod} = 0.8$ slow down the equilibration of the diffusion in the metaplex (the circles are over the crosses in Figure 17b.) The same results are reproduced when a much bigger value of $s_{net} = 4$ is used, as can be seen in Figures 17c and 17d.

The reason for this apparently counterintuitive behavior has been previously discussed for the toy model: in a small node it is counterproductive to make long jumps inside the node. The reason is that the diffusive particle will rarely find the sink to escape from the node. In a similar fashion, inside a big node it is counterproductive to make small jumps as it will slow down the mobility of particles away from the source to reach the sink and leave the node. We again conclude that the size of the nodes influences the global dynamics of the metaplex. Also importantly, the nature of the internal structure can change significantly the rate of convergence of the process and can make it faster or slower depending of the size of the nodes and the nature of the diffusive process inside them.

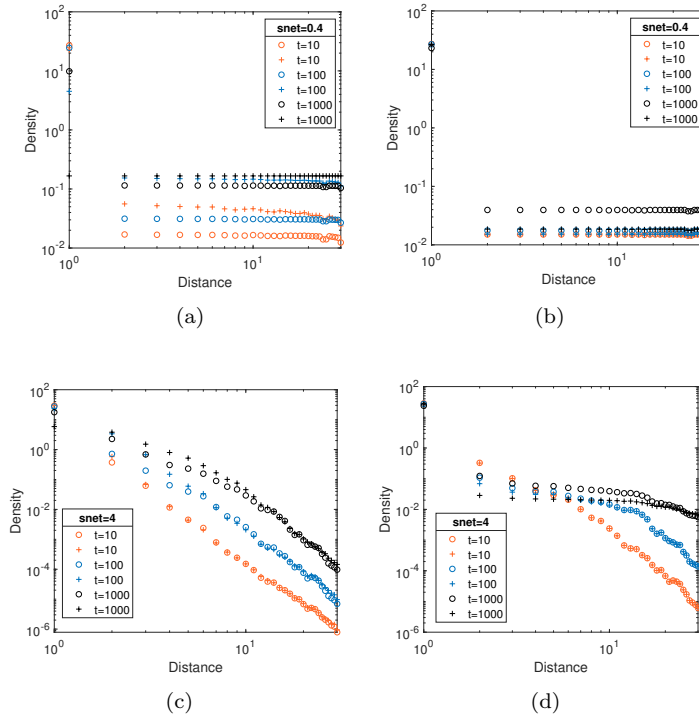


FIG. 17. *Density as a function of distance for disjoint coupling points and $s_{nod} = 0.8$ (+), $s_{nod} = 0.2$ (o). (a) and (c) correspond to Ω_s and (b) and (d) correspond to Ω_b .*

Let us now consider the combined influence of the endo- and exo-dynamics on the global metaplex diffusion. We start here by considering the time evolution of the diffusive particle across the metaplex after initiating the process at a randomly selected node.

In Figure 18a we illustrate the time evolution of the density (in logarithmic scale)

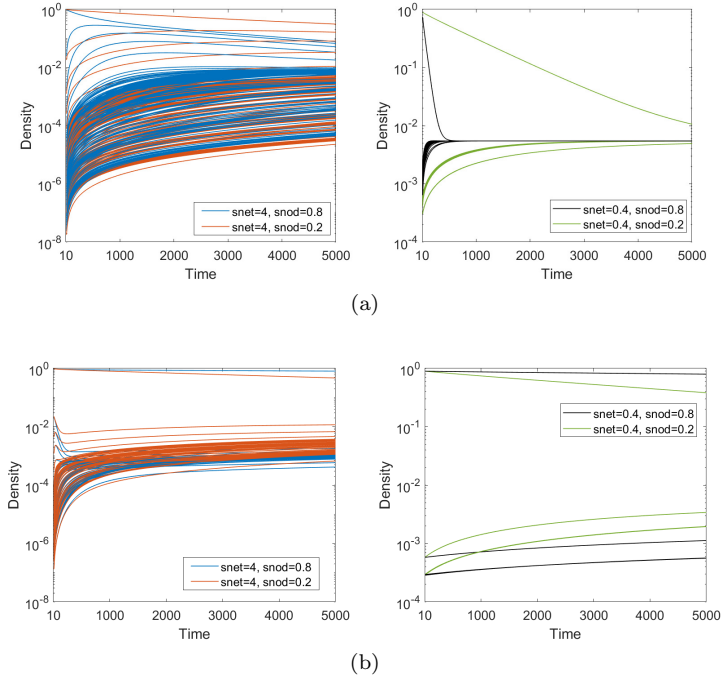


FIG. 18. Time evolution of the diffusion dynamics for Ω_s (a) and Ω_b (b) with disjoint sink and sources inside the node of the landscape metaplex.

of the diffusive particle. In the left panel of Figure 18a we observe that the diffusion with $s_{nod} = 0.8$ converges to the steady state at an earlier time than that for $s_{nod} = 0.2$ when the same value of $s_{net} = 4$ is used. The same is observed, even clearer, in the right panel where the process for $s_{nod} = 0.8$ and $s_{net} = 0.4$ converges significantly faster to the steady state than that for $s_{nod} = 0.2$ and $s_{net} = 0.4$. See Table 1 for the values of the standard deviation introduced in Section 2.

	$s_{net} = 4$		$s_{net} = 0.4$	
	$s_{nod} = 0.2$	$s_{nod} = 0.8$	$s_{nod} = 0.2$	$s_{nod} = 0.8$
Ω_s	0.0265	0.0088	$3.9 \cdot 10^{-4}$	$1.8 \cdot 10^{-11}$
Ω_b	0.034	0.059	0.028	0.059

TABLE 1
Standard deviation at $t = 5000$ for the landscape metaplex

Making the nodes bigger shows the same behaviour as discussed above. The slower dynamics, compared to the small nodes, (see Figure 18b) is expected from the fact that now the diffusive particle has more area to diffuse before finding the way out of the node. However, the most interesting observation is that now, as we have previously pointed out, the order of convergence rates is reversed. For the bigger node, the global diffusion equilibrates faster when we have superdiffusion inside the nodes than when $s_{nod} = 0.8$ (compare values in Table 1 for Ω_b). Similar results are observed for the case $s_{net} = 0.4$.

From Figure 18a we observe that varying s_{net} and s_{nod} changes the rate of convergence of the diffusion in the metaplex. So we conclude that, although the landscape

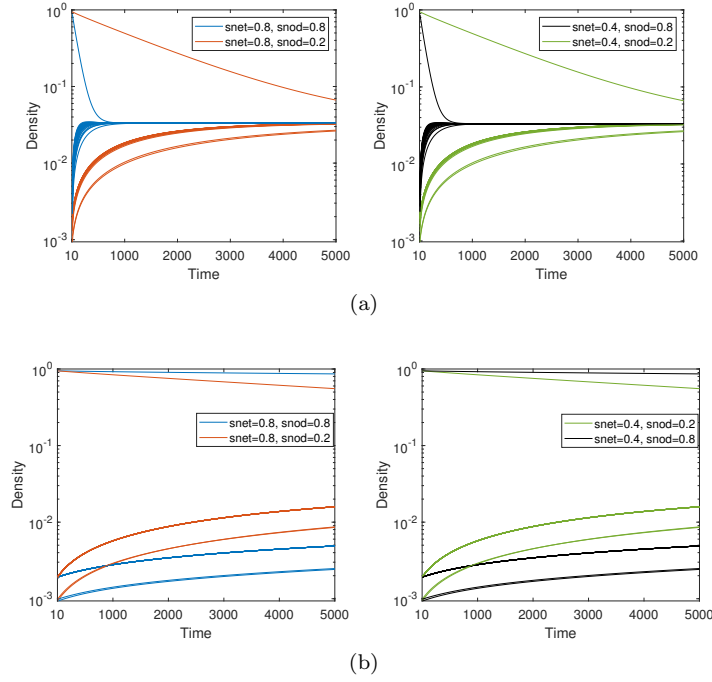


FIG. 19. Time evolution of the diffusion process on the macaque visual cortex metaplex using different parameters for the endo- and exo-dynamics (see text for details).

metaplex has a large-world exo-skeleton, it displays a trade-off between the exo- and endo-dynamics that determines the global convergence of the diffusion in the metaplex. It is neither the exo-structure nor the endo-structure alone, but a complex interrelation of both which controls the global dynamics in the metaplex.

7.2. Visual cortex metaplex of macaque. The second metaplex consists of 30 regions of the macaque visual cortex. These cortex regions are functionally connected by 190 edges, which makes the exo-structure of this system very dense, with density $\delta \approx 0.437$. As a consequence of this high edge density the network is a “ultra-small-world” with average shortest path distance between cortex regions of $\bar{d} \approx 1.54$ and a maximum separation between two of these regions of only $d_{max} = 3$ steps. This makes the exo-skeleton of this metaplex a “ultra-small-world”. The average degree is approximately 12.67 with a maximum number of connections at a given node is 22.

This network displays an almost uniform degree distribution, particularly for degrees between 4 and 16. Therefore, we just pick at random the nodes to initiate the diffusion on the metaplex as most of the nodes are degree-equivalent. We then proceed with a similar analysis as for the case of the landscape metaplex by studying the effects of the endo- and exo-dynamics on the global diffusion.

When the nodes are small, Figure 19a, we observe the same effect as in the previous cases, namely that larger values of s_{nod} favor the convergence of the dynamics to the steady state (see Table 2 for the standard deviation values). The results for the big nodes (Figure 19b) are similar as for the toy model and landscape metaplex, i.e., superdiffusion inside the nodes favors the convergence of the dynamics to the steady state.

	$s_{net} = 0.8$		$s_{net} = 0.4$	
	$s_{nod} = 0.2$	$s_{nod} = 0.8$	$s_{nod} = 0.2$	$s_{nod} = 0.8$
Ω_s	0.0064	$1.378 \cdot 10^{-9}$	0.0064	$1.3283 \cdot 10^{-9}$
Ω_b	0.0983	0.1567	0.0983	0.1567

TABLE 2

Standard deviation at $t = 5000$ for the macaque visual cortex metaplex

For the macaque visual cortex metaplex the change of s_{net} practically changes nothing in the global dynamics. For instance, we see from [Figure 19a](#) that keeping constant $s_{nod} = 0.8$ and dropping s_{net} from 0.8 (blue lines in the left panel) to $s_{net} = 0.4$ (black lines in the right panel) almost leaves unaffected the time evolution of the diffusion. The standard deviations at $t = 5000$ time units are in [Table 2](#). We observe a similar behaviour for the case of big nodes (see [Figure 19b](#)).

These results are in clear contrast with the ones previously discussed for the landscape metaplex. In the previous case it was observed a trade-off between the exo- and endo-dynamics to control the global diffusion at the metaplexic scale. Here, the exo-dynamics does not play any significant role in the global dynamics of the metaplex. The factor which determines such global dynamics is the endo-structure of the nodes in the metaplex. The reasons for this extreme case of dependence of the global dynamics almost exclusively is two-fold. Firstly, the exo-skeleton of the macaque visual cortex analyzed here is an ultra-small-world, where long range hops are not possible. The second is the almost-complete nature of this exo-structure, i.e., its high density and uniformity of degree distribution. It is intuitively clear that in a complete network there are no topological effects that can affect the dynamics. In this case only the endo-dynamics has a significant influence on the metaplexic global dynamics.

Most real-world metaplexes are expected to have exo-structures which are not so dense and uniform as the one of the macaque visual cortex. Although they certainly display small-world properties, they show a larger variability of shortest path distances than the macaque cortex. Thus, it is expected that they display certain trade-off between the endo- and the exo-structures like the one observed here for the landscape metaplex in determining the global dynamics of the system.

8. Summary. The concept of metaplex introduced in this work allows to study the trade-off between the internal structure and dynamics of/in the nodes. Here we provide the basic notions and motivations for the study of metaplexes with continuous internal structure of the nodes and discrete inter-node dynamics. Additionally, we provide theoretical and computational support for a series of results related to the study of diffusive dynamics on metaplexes. In particular, we present examples in which the endo structure of the metaplex determines almost uniquely the global dynamics: in the macaque visual cortex the exo-structure plays no fundamental role. On the other hand, in the linear metaplex chain there is a trade-off between the endo- and exo-dynamics to determine the global diffusion. This is reflected in the Madagascar metaplex landscape. We have also studied here the effect of the geometry, such as the size of nodes, location of sink and sources, and the nature and strength of the coupling between nodes.

Our numerical results show that superdiffusion due to long range hopping in the linear network $\mathcal{Q} = \{\dots, -2, -1, 0, 1, 2, \dots\}$, as in [\[22\]](#), survives irrespective of the internal structure of the nodes ([Figure 13](#)). The parameter range of Mellin exponents

for which superdiffusion is observed, $s_{net} \in (1, 3)$, is the same as for ordinary networks of point nodes without internal structure. The conclusion extends to certain networks from applications, of a large diameter, here studied for the landscape network of habitats of *L. catta* (Figure 17). The combine influence of the endo- and exo-structure determined the global diffusion in such networks.

The endo-structure, on the other hand, dominates at shorter distances and therefore becomes crucial for diffusion in small-world metaplexes. This was illustrated for the cortical metaplex of the macaque, Figure 19. The effect of the internal dynamics in the whole metaplex strongly depends on the geometry of the nodes and the nature of the coupling. When sinks and sources overlap, internal superdiffusion may *slow down* the metaplex dynamics, and normal diffusion is faster on small scales. When sinks and sources are in separate, distant locations, superdiffusion in the nodes allows particles to explore the entire metaplex much faster than classical diffusion. While it accelerates diffusion, the internal superdiffusion cannot, by itself, induce superdiffusion in the metaplex.

Our results can be understood from the local description we provide of the distribution of particles inside each node. The combination of analytical methods for the PDE description in the node, and network methods for their interconnection in the exo-skeleton gives a new perspective not only on classical complex network descriptions, but also for the study of PDEs describing physical systems which can be either split into continuous regions interconnected in a discrete way or involve a network of internal degrees of freedom. This illustrates how the study of metaplexes will draw tools from a wide range of areas, such as the geometric analysis of coupled PDEs and interface problems, spectral theory of operator matrices, high-dimensional stochastic processes etc. Conversely, it suggests the relevance of network theory for old problems in these fields, such as the problem of finding effective descriptions of interacting many-particle systems with high-dimensional internal degrees of freedom.

From a computational point of view, numerical experiments for large metaplexes become a challenge, due to the new internal degrees of freedom in each node. For applications to real-world networks, future work should explore methods which represent this internal dynamics efficiently. Model order reduction or generalized finite element methods [52] are examples which have been used in related settings to achieve a reasonable accuracy already for small degrees of freedom.

REFERENCES

- [1] Frederic Bartumeus, P Fernández, MGE da Luz, Jordi Catalan, Ricard V Solé, and Simon A Levin. Superdiffusion and encounter rates in diluted, low dimensional worlds. *The European Physical Journal Special Topics*, 157(1):157–166, 2008.
- [2] Jean Bertoin. *Lévy Processes*. Cambridge University Press, 1998.
- [3] Stefano Boccaletti, Ginestra Bianconi, Regino Criado, Charo I Del Genio, Jesús Gómez-Gardenes, Miguel Romance, Irene Sendia-Nadal, Zhen Wang, and Massimiliano Zanin. The structure and dynamics of multilayer networks. *Physics Reports*, 544(1):1–122, 2014.
- [4] Stefano Boccaletti, Vito Latora, Yamir Moreno, Martin Chávez, and D-U Hwang. Complex networks: Structure and dynamics. *Physics Reports*, 424(4-5):175–308, 2006.
- [5] Örjan Bodin and Jon Norberg. A network approach for analyzing spatially structured populations in fragmented landscape. *Landscape Ecology*, 22(1):31–44, 2007.
- [6] Örjan Bodin, Maria Tengö, Anna Norman, Jakob Lundberg, and Thomas Elmqvist. The value of small size: loss of forest patches and ecological thresholds in southern madagascar. *Ecological applications*, 16(2):440–451, 2006.
- [7] Jean-Philippe Bouchaud and Antoine Georges. Anomalous diffusion in disordered media: statistical mechanisms, models and physical applications. *Physics reports*, 195(4-5):127–293, 1990.

- [8] Ed Bullmore and Olaf Sporns. Complex brain networks: graph theoretical analysis of structural and functional systems. *Nature Reviews Neuroscience*, 10(3):186, 2009.
- [9] JF Burrow, PD Baxter, and JW Pitchford. Lévy processes, saltatory foraging, and superdiffusion. *Mathematical Modelling of Natural Phenomena*, 3(3):115–130, 2008.
- [10] Xi Chen, Liang Guo, Jianhong Kang, Yunlong Huo, Shiqiang Wang, and Wenchang Tan. Calcium waves initiating from the anomalous subdiffusive calcium sparks. *Journal of The Royal Society Interface*, 11(91):20130934, 2014.
- [11] AH Cornell-Bell and SM Finkbeiner. Ca^{2+} waves in astrocytes. *Cell calcium*, 12(2-3):185–204, 1991.
- [12] Tommaso Costa, Giuseppe Boccignone, Franco Cauda, and Mario Ferraro. The foraging brain: evidence of levy dynamics in brain networks. *PloS one*, 11(9):e0161702, 2016.
- [13] Richard Courant and David Hilbert. *Methods of Mathematical Physics: Partial Differential Equations*. John Wiley & Sons, 2008.
- [14] Serena Dipierro, Xavier Ros-Oton, and Enrico Valdinoci. Nonlocal problems with Neumann boundary conditions. *Revista Matemática Iberoamericana*, 33(2):377–416, 2017.
- [15] Jonathan F Donges, Yong Zou, Norbert Marwan, and Jürgen Kurths. Complex networks in climate dynamics. *The European Physical Journal Special Topics*, 174(1):157–179, 2009.
- [16] Makoto Endo, Minoru Tanaka, and Yasuo Ogawa. Calcium induced release of calcium from the sarcoplasmic reticulum of skinned skeletal muscle fibres. *Nature*, 228(5266):34, 1970.
- [17] Radek Erban and Hans G Othmer. From individual to collective behavior in bacterial chemotaxis. *SIAM Journal on Applied Mathematics*, 65(2):361–391, 2004.
- [18] Radek Erban and Hans G Othmer. From signal transduction to spatial pattern formation in e. coli: a paradigm for multiscale modeling in biology. *Multiscale Modeling & Simulation*, 3(2):362–394, 2005.
- [19] Ernesto Estrada. Path laplacian matrices: introduction and application to the analysis of consensus in networks. *Linear Algebra and its Applications*, 436(9):3373–3391, 2012.
- [20] Ernesto Estrada. *The structure of complex networks: theory and applications*. Oxford University Press, 2012.
- [21] Ernesto Estrada and Örjan Bodin. Using network centrality measures to manage landscape connectivity. *Ecological Applications*, 18(7):1810–1825, 2008.
- [22] Ernesto Estrada, Ehsan Hameed, Naomichi Hatano, and Matthias Langer. Path Laplacian operators and superdiffusive processes on graphs. I. One-dimensional case. *Linear Algebra and its Applications*, 523:307–334, 2017.
- [23] Ernesto Estrada, Ehsan Hameed, Matthias Langer, and Aleksandra Puchalska. Path laplacian operators and superdiffusive processes on graphs. ii. two-dimensional lattice. *Linear Algebra and its Applications*, 555:373–397, 2018.
- [24] Gissell Estrada-Rodriguez, Heiko Gimperlein, Kevin J Painter, and Jakub Stoczek. Space-time fractional diffusion in cell movement models with delay. *Mathematical Models and Methods in Applied Sciences*, 29:65–88, 2019.
- [25] Alexandre Fabiato and Francoise Fabiato. Excitation-contraction coupling of isolated cardiac fibers with disrupted or closed sarcolemmas: calcium-dependent cyclic and tonic contractions. *Circulation Research*, 31(3):293–307, 1972.
- [26] Erwin Frey and Klaus Kroy. Brownian motion: a paradigm of soft matter and biological physics. *Annalen der Physik*, 14(1-3):20–50, 2005.
- [27] Jianxi Gao, Sergey V Buldyrev, Shlomo Havlin, and H Eugene Stanley. Robustness of a network of networks. *Physical Review Letters*, 107(19):195701, 2011.
- [28] Heiko Gimperlein and Gerd Grubb. Heat kernel estimates for pseudodifferential operators, fractional Laplacians and Dirichlet-to-Neumann operators. *Journal of Evolution Equations*, 14(1):49–83, Mar 2014.
- [29] Ido Golding and Edward C Cox. Physical nature of bacterial cytoplasm. *Physical Review Letters*, 96(9):098102, 2006.
- [30] Sergio Gómez, Albert Diaz-Guilera, Jesus Gómez-Gardenes, Conrad J Pérez-Vicente, Yamir Moreno, and Alex Arenas. Diffusion dynamics on multiplex networks. *Physical Review Letters*, 110(2):028701, 2013.
- [31] Joaquín Goñi, Gonzalo Arrondo, Jorge Sepulcre, Inigo Martincorena, Nieves Vélez de Mendizábal, Bernat Corominas-Murtra, Bartolomé Bejarano, Sergio Ardanza-Trevijano, Herminia Peraita, Dennis P Wall, et al. The semantic organization of the animal category: evidence from semantic verbal fluency and network theory. *Cognitive processing*, 12(2):183–196, 2011.
- [32] Alexander Grigor’yan. Heat kernels and function theory on metric measure spaces. in: *Heat kernels and analysis on manifolds, graphs, and metric spaces (Paris, 2002)*, *Contemp. Math.* 338, Amer. Math. Soc., Providence, RI, pages 143–172, 2003.

- [33] Thomas T Hills. Animal foraging and the evolution of goal-directed cognition. *Cognitive science*, 30(1):3–41, 2006.
- [34] WK Jo, ACK Law, and SK Chung. The neglected co-star in the dementia drama: the putative roles of astrocytes in the pathogenesis of major neurocognitive disorders. *Molecular Psychiatry*, 19(2):159, 2014.
- [35] Boris S Kerner. *The physics of traffic: empirical freeway pattern features, engineering applications, and theory*. Springer, 2012.
- [36] Mikko Kivelä, Alex Arenas, Marc Barthélemy, James P Gleeson, Yamir Moreno, and Mason A Porter. Multilayer networks. *Journal of Complex Networks*, 2(3):203–271, 2014.
- [37] M Köpf, C Corinthe, O Haferkamp, and TF Nonnenmacher. Anomalous diffusion of water in biological tissues. *Biophysical Journal*, 70(6):2950–2958, 1996.
- [38] Hendrik Anthony Kramers. Brownian motion in a field of force and the diffusion model of chemical reactions. *Physica*, 7(4):284–304, 1940.
- [39] Edward G Lakatta and Thomas Guarnieri. Spontaneous myocardial calcium oscillations: are they linked to ventricular fibrillation? *Journal of Cardiovascular Electrophysiology*, 4(4):473–489, 1993.
- [40] Vito Latora, Vincenzo Nicosia, and Giovanni Russo. *Complex networks: principles, methods and applications*. Cambridge University Press, 2017.
- [41] Melvin Lax, Wei Cai, and Min Xu. *Random processes in physics and finance*. Oxford University Press, 2006.
- [42] Luyao Lu, Ling Xia, Xuesong Ye, and Heping Cheng. Simulation of the effect of rogue ryanodine receptors on a calcium wave in ventricular myocytes with heart failure. *Physical Biology*, 7(2):026005, 2010.
- [43] Katherine Luby-Phelps. Cytoarchitecture and physical properties of cytoplasm: volume, viscosity, diffusion, intracellular surface area. In *International review of cytology*, volume 192, pages 189–221. Elsevier, 1999.
- [44] Franziska Matthäus, Marko Jagodič, and Jure Dobnikar. E. coli superdiffusion and chemotaxis-search strategy, precision, and motility. *Biophysical Journal*, 97(4):946–957, 2009.
- [45] D M McAvity and H Osborn. A DeWitt expansion of the heat kernel for manifolds with a boundary. *Classical and Quantum Gravity*, 8(4):603, 1991.
- [46] Ralf Metzler and Joseph Klafter. The random walk’s guide to anomalous diffusion: a fractional dynamics approach. *Physics Reports*, 339(1):1–77, 2000.
- [47] Ralf Metzler and Joseph Klafter. The restaurant at the end of the random walk: recent developments in the description of anomalous transport by fractional dynamics. *Journal of Physics A: Mathematical and General*, 37(31):R161, 2004.
- [48] Maiken Nedergaard, Bruce Ransom, and Steven A Goldman. New roles for astrocytes: redefining the functional architecture of the brain. *Trends in Neurosciences*, 26(10):523–530, 2003.
- [49] Mark E J Newman. The structure and function of complex networks. *SIAM Review*, 45(2):167–256, 2003.
- [50] Charles Nicholson. Diffusion and related transport mechanisms in brain tissue. *Reports on Progress in Physics*, 64(7):815, 2001.
- [51] Dan V Nicolau Jr, John F Hancock, and Kevin Burrage. Sources of anomalous diffusion on cell membranes: a monte carlo study. *Biophysical Journal*, 92(6):1975–1987, 2007.
- [52] Patrick O’Hara, C. Armando Duarte, and Thomas Eason. Transient analysis of sharp thermal gradients using coarse finite element meshes. *Computer Methods in Applied Mechanics and Engineering*, 200(5-8):812–829, 2011.
- [53] El-Maati Ouhabaz. *Analysis of heat equations on domains.(LMS-31)*. Princeton University Press, 2009.
- [54] Benoît Perthame, Weiran Sun, and Min Tang. The fractional diffusion limit of a kinetic model with biochemical pathway. *Zeitschrift für angewandte Mathematik und Physik*, 69(3):67, 2018.
- [55] Mason A Porter. What is ... a multilayer network. *Notices of the AMS*, 11:1419–1423, 2018.
- [56] Julia F Revere, Jae-Hyung Jeon, Han Bao, Matthias Leippe, Ralf Metzler, and Christine Selhuber-Unkel. Superdiffusion dominates intracellular particle motion in the supercrowded cytoplasm of pathogenic *acanthamoeba castellanii*. *Scientific Reports*, 5:11690, 2015.
- [57] Ellis B Ridgway, John C Gilkey, and Lionel F Jaffe. Free calcium increases explosively in activating medaka eggs. *Proceedings of the National Academy of Sciences*, 74(2):623–627, 1977.
- [58] Hugo Sanabria, Yoshihisa Kubota, and M Neal Waxham. Multiple diffusion mechanisms due to nanostructuring in crowded environments. *Biophysical Journal*, 92(1):313–322, 2007.
- [59] Comandur Seshadhri, Tamara G Kolda, and Ali Pinar. Community structure and scale-free

- collections of erdős-rényi graphs. *Physical Review E*, 85(5):056109, 2012.
- [60] Stephen Smith, Claudia Cianci, and Ramon Grima. Macromolecular crowding directs the motion of small molecules inside cells. *Journal of The Royal Society Interface*, 14(131):20170047, 2017.
 - [61] Albert Sole-Ribalta, Manlio De Domenico, Nikos E Kouvaris, Albert Diaz-Guilera, Sergio Gómez, and Alex Arenas. Spectral properties of the Laplacian of multiplex networks. *Physical Review E*, 88(3):032807, 2013.
 - [62] Christiane Tretter. *Spectral theory of block operator matrices and applications*. World Scientific, 2008.
 - [63] Dean Urban and Timothy Keitt. Landscape connectivity: a graph-theoretic perspective. *Ecology*, 82(5):1205–1218, 2001.
 - [64] GM Viswanathan, Frederic Bartumeus, Sergey V Buldyrev, Jordi Catalan, UL Fulco, Shlomo Havlin, MGE Da Luz, Marcelo Leite Lyra, EP Raposo, and H Eugene Stanley. Lévy flight random searches in biological phenomena. *Physica A: Statistical Mechanics and Its Applications*, 314(1-4):208–213, 2002.
 - [65] Stephanie C. Weber, Andrew J. Spakowitz, and Julie A. Theriot. Bacterial chromosomal loci move subdiffusively through a viscoelastic cytoplasm. *Phys. Rev. Lett.*, 104:238102, Jun 2010.
 - [66] Jonathon Wetherington, Geidy Serrano, and Ray Dingledine. Astrocytes in the epileptic brain. *Neuron*, 58(2):168 – 178, 2008.
 - [67] Kazuko Yamasaki, Avi Gozolchiani, and Shlomo Havlin. Climate networks around the globe are significantly affected by el nino. *Physical review letters*, 100(22):228501, 2008.
 - [68] Damián H Zanette. Statistical-thermodynamical foundations of anomalous diffusion. *Brazilian journal of physics*, 29(1):108–124, 1999.
 - [69] Huan-Xiang Zhou, Germn Rivas, and Allen P. Minton. Macromolecular crowding and confinement: Biochemical, biophysical, and potential physiological consequences. *Annual Review of Biophysics*, 37(1):375–397, 2008. PMID: 18573087.
 - [70] Steven B. Zimmerman and Stefan O. Trach. Estimation of macromolecule concentrations and excluded volume effects for the cytoplasm of escherichia coli. *Journal of Molecular Biology*, 222(3):599 – 620, 1991.